AGU PUBLICATIONS

Geophysical Research Letters

Supporting Information for

D/H Isotope Ratios In The Global Hydrologic Cycle

Stephen P. Good[1,2], David Noone[3], Naoyuki Kurita[4], Marion Benetti[5], Gabriel J. Bowen[1]

1) University of Utah, Department of Geology and Geophysics, Salt Lake City, Utah, USA

2) Department of Biological and Ecological Engineering, Oregon State University, Corvallis, Oregon, USA

3) College of Earth, Ocean and Atmospheric Sciences, Oregon State University, Corvallis, Oregon, USA

4) Graduate School of Environmental Studies, Nagoya University, Nagoya, Japan

5) Laboratoire d'Ocanographie et du Climat, Exprimentations et approches Numriques, IPSL, UPMC, CNRS, Paris, France

Contents of this file

Additional Supporting Information (Files uploaded separately)

Dataset S1

Introduction

This Supporting Information file contains supplementary Text S1, Text S2, Text S3, and Text S4, Figures S1 and S2, Tables S1 and S2, Captions for Dataset S1, and references. Text S1 though S4 describe the data analysis methodology of this study. Figure S1 shows the differences between ship based observations of δ_A and Tropospheric Emissions Spectrometer (TES) δ_A estimates before and after applying the calibration correction and Figure S2 is a flowchart depicting data analysis. Table S1 lists the TES calibration coefficients used to correct the satellite retrievals. Table S2 and S3 document literature reviews of measurements of the D/H ratio of the world's major rivers and in evapotranspiration flux estimates respectively. Dataset S1 includes monthly bias-corrected estimates of δ_A and associated uncertainties.

Text S1

Multivariate Regression

This study used data from the Tropospheric Emissions Spectrometer (TES), specifically the latest version of the TES Lite products (v006) which report HDO, H_2O, and a suite of other meta-data on 17 pressure levels. Spectral radiance is measured by TES in the 650 to 3050 cm^{-1} (15.4 to 3.3 μm) bands at an apodized resolution of 0.1 cm^{-1}. A correction is applied to each individual TES retrieval to estimate the surface vapor D/H isotope ratio. The applied correction takes the form of

$$\text{(S1)} \qquad \delta_A = \beta_1 x_1 + \beta_2 x_2 + \cdots + \beta_{n-1} x_{n-1} + \beta_n + \varepsilon,$$

where δ_A is the corrected surface composition, β_1 through $\beta_{n\text{-}1}$ are the correction coefficients, x_1 through $x_{n\text{-}1}$ are the regression parameters respectively, β_n is the final intercept term, and ε is the random error not captured by this regression (further described in **Text S4**).

Throughout this study, all D/H isotope ratios are reported relative to the V-SMOW standard in δ notation expressed in parts per thousand (‰=10^{-3}), where $\delta = R_{\text{sample}}/R_{\text{std}} - 1$, with R the ratio of D to H. The TES surface layer is defined as the average of the bottom two pressure levels within the TES lite data files and troposphere values are calculated as the average of all levels (including the surface) below the tropopause. The two TES layers used in this analysis reflects vapor at an average pressure of 996hPA, which corresponds to the lowermost ~140m of the atmosphere. We found that two layers, while integrating over a thicker layer, provided improved performance over using just the lower most TES layer alone.

The chosen regression parameters (listed in **Table S1**) represent a compromise between parsimonious model development and accurate estimation. Though a single isotope profile as a function of pressure is used as the TES a-priori [*Herman and Osterman*, 2012], variations in surface and tropopause pressure will cause values both these a-prioi isotope values to vary for each retrieval, thus capturing many physical atmospheric processes that control the quality of the TES retrieval. Similarly, variation in water vapor mixing ratios (q) at both the surface and within the entire troposphere will also alter the quality of the TES retrieval [*Field et al.*, 2012]. Other properties of the TES retrieval, such as the surface temperature, nadir angle, and the values within the TES averaging kernel, were also found to be strongly correlated with the TES HDO bias relative to the ship based δ_A values. However, many of these were redundant with the parameters listed in **Table S1** and were therefore not included in the bias-correction model developed here, though they merit further investigation.

The best fit and associated uncertainty in values of correction coefficients (β's) was determined though a multivariate least squares regression where δ_A in equation (S1) is taken to be the data set of the ship based observations. A jackknifing approach [*Wu*, 1986; *Bowen and Revenaugh*, 2003] is used to assess the uncertainty in the regression, wherein each ship based observation is removed from the data set, and a regression is preformed to determine the β values. The mean and standard deviation (σ_n) of these different regression models were then calculated and shown in **Table S1**. Before applying the correction, the mean difference between δ_A observed from the ships and δ_A observed from TES was 14.5‰ (red histogram

Figure S1). Cross-validation of the bias-corrected results using the jackknife iterations (each observation was removed and the compared with the predicted value at that site using the newly derived set of β values) shows that the average prediction bias is removed (blue histogram Figure S1). Also shown in **Table S1** are the Pearson correlation coefficients between δ_A observed from the ship and each regression parameter.

Text S2

Oceanic Evaporation Isotopic Composition

The isotopic composition of oceanic evaporation flux, $\delta_{E(O)}$, is calculated based on the ratio of the HDO vapor pressure deficit to the H_2O vapor pressure deficit [*Craig and Gordon*, 1965] as

$$\delta_{E(O)} = \frac{\alpha_* \delta_L - h\delta_A - (\varepsilon_* + \varepsilon_K)}{(1-h) + 10^{-3}\varepsilon_K}. \tag{S2}$$

Above, sea surface water isotopic composition, δ_L, is assumed equal to 0, and surface vapor composition, δ_A, is estimated based on the bias-corrected climatologically averaged TES observations (Text S1). The vapor/liquid equilibrium fractionation factor, α_*, is dependent on surface temperature [*Majoube*, 1971], and the equilibrium enrichment is given by $\varepsilon_*=(1-\alpha_*)10^3$. The value of the kinetic enrichment, $\varepsilon_K=C_K(1-h)$, is determined by surface conditions and is not well constrained, and therefore we conservatively assume that C_K ranges from 2 to 6.5, representing the range of values expected for rough to smooth oceanic conditions [*Merlivat and Jouzel*, 1979]. Both temperature and surface-normalized relative humidity, *h*, are obtained directly from the TES retrievals and averaged within each grid cell in the same manner as the δ_A values [*Gat*, 1996; *Horita et al.*, 2008].

Text S3

Atmospheric and Oceanic Mass Fluxes

A total mass flux is calculated for oceanic evaporation, total oceanic precipitation, total land precipitation and the associated isotopologue fluxes. Total land evapotranspiration and runoff, and their associated isotopic values are then determined as the residuals of the atmosphere and ocean mass balance. Values for oceanic evaporation isotope composition were calculated as described above (**Text S2**) while data from global the Global Network of Isotopes in Precipitation (GNIP) and published literature were used to model global precipitation isotope values (δ_P) based on a non-linear least squares approach [*Bowen and Wilkinson*, 2002; *Bowen and Revenaugh*, 2003]. Briefly, this method involves optimization of a model representing observed δ_P as a function of site latitude and elevations (as proxies for temperature effects) and a interpolated spatial field of residuals from the latitude-elevation model (reflecting circulation-driven effects). The accuracy of this approach has been determined via resampling (*N*-1 Jackknife), at stations and resulted an average error of ~9.4‰ [*Bowen and Revenaugh*, 2003]. The set of Jackknifed model parameters were used to generate a synthetic set of grids representing precipitation isotopic composition for each month and its uncertainty.

The mean global precipitation over land, $\overline{P(L)}$, and its associated isotopic value, $\overline{\delta_{P(L)}}$, are estimated as

(S3a) $$\overline{P(L)} = \sum_{m,x,y} P(m,x,y)A(x,y)I(x,y)$$

and

(S3b) $$\overline{\delta_{P(L)}} = \frac{\sum_{m,x,y} \delta_P(m,x,y)P(m,x,y)A(x,y)I(x,y)}{\sum_{m,x,y} P(m,x,y)A(x,y)I(x,y)}.$$

Where $P(m,x,y)$ is the average precipitation occurring in grid cell at location *x, y,* in month *m* taken from the GPCP [*Adler et al.*, 2003]. The indicator function, $I(x,y)$, takes a value of 1 if the current grid cell is over land or a value of 0 if over water, and $A(x,y)$ is the area of each 2x2 degree grid cell. Similarly, the mean global precipitation over the oceans, $\overline{P(O)}$, and its associated isotopic composition, $\overline{\delta_{P(O)}}$, are estimated as

(S4a) $$\overline{P(O)} = \sum_{m,x,y} P(m,x,y)A(x,y)(1-I(x,y))$$

and

(S4b)
$$\overline{\delta_{P(O)}} = \frac{\sum_{m,x,y} \delta_P(m,x,y)P(m,x,y)A(x,y)(1-I(x,y))}{\sum_{m,x,y} P(m,x,y)A(x,y)(1-I(x,y))}.$$

Finally, calculation of mean global evaporation over the oceans, $\overline{E(O)}$, and its associated isotopic composition, $\overline{\delta_{E(O)}}$, are estimated as

(S5a)
$$\overline{E(O)} = \sum_{m,x,y} E(m,x,y)A(x,y)(1-I(x,y))$$

and

(S5b)
$$\overline{\delta_{E(O)}} = \frac{\sum_{m,x,y} \delta_{E(O)}(m,x,y)E(m,x,y)A(x,y)(1-I(x,y))}{\sum_{m,x,y} E(m,x,y)A(x,y)(1-I(x,y))}.$$

Where $E(m,x,y)$ is evaporation occurring in each grid cell each month [*Yu and Weller*, 2007].

Atmospheric and Oceanic Mass Balance

Based on the estimated global fluxes and their associated isotopic composition, we construct a mass balance of the Earths oceans and atmosphere for both H_2O and HDO. These are used to estimate the isotopic composition of global continental runoff, $\overline{\delta_{R(L)}}$, and global continental evapotranspiration, $\overline{\delta_{ET(L)}}$. The mass balance of the oceans is solved for global runoff isotopic composition as

(S6)
$$\overline{\delta_{R(L)}} = \frac{\overline{\delta_{E(O)}}\,\overline{E(O)} - \overline{\delta_{P(O)}}\,\overline{P(O)}}{\overline{E(O)} - \overline{P(O)}},$$

where the denominator on the right side in Equation S6 is the global runoff flux amount. Similarly, we construct a mass balance of the atmosphere and solve for the isotopic composition of land evapotranspiration as

(S7)
$$\overline{\delta_{ET(L)}} = \frac{\overline{\delta_{P(O)}}\,\overline{P(O)} + \overline{\delta_{P(L)}}\,\overline{P(L)} - \overline{\delta_{E(O)}}\,\overline{E(O)}}{\overline{P(O)} + \overline{P(L)} - \overline{E(O)}},$$

where the denominator on the right hand side in Equation S7 is the global continental evapotranspiration flux amount.

Text S4

Monte-Carlo Simulations of Fluxes

An ensemble of Monte-Carlo simulations is used to determine uncertainty in the final estimate of $\overline{\delta_{R(L)}}$ and $\overline{\delta_{ET(L)}}$, with the workflow depicted in **Figure S2**. In total 1000 different simulations were conducted, each resulting in a unique value of $\overline{\delta_{R(L)}}$ and $\overline{\delta_{ET(L)}}$, with the mean and standard deviation of these 1000 values taken as our final result.

The first step, as described in **Text S1**, was to use the each of the *N-1* jackknife regression to determine the mean and covariance matrix the regression coefficients. Then, for each simulation, a set of regression coefficients was randomly generated assuming a bivariate normal distribution for these parameters. This set of regression coefficients was then use to estimate a bias-corrected value of δ_A for each TES retrieval. After applying our bias-correction the difference between the observed $\delta_{A(Ship)}$ value and the corrected TES $\delta_{A(Cor)}$ has an average value of zero, denoting that the bias has been removed, and a standard deviation of 13.4‰ (**Figure S1).** This residual uncertainty not captured with the multivariate regression is propagated by adding random noise, ε (i.e. an independent and identically distributed random variable) with mean zero and standard deviation σ_ε=13.4‰ to each retrieval for each Monte-Carlo simulation (first and second red box in **Figure S2**). Thus in each grid cell the standard deviation of $\delta_{A(Cor)}$ between Monte-Carlo simulations will decrease with 1/sqrt(*N*), with *N* the number of TES retrievals in each grid cell (See Figure 2A and 2B of the main article). Similarly, random perturbations to the TES values of surface temperature and relative humidity were added independently to each TES retrieval in each simulation for the TES. For temperature a normal distribution of errors was assumed with a standard deviation of 2 degrees C (third red box in **Figure S2**), while for relative humidity a Beta distribution (bound at 0 and 1) about the TES retrieved value was assumed with a standard deviation of 10% RH (fourth red box in **Figure S2**).

TES data from 2005 though 2012 was used, and each month contained approximately 30,000 TES retrievals for δ_A, surface temperature and normalized relative humidity each month, and all of these retrievals were simulated 1000 times with uncertainty added to each unique value separately (third row in **Figure S2**). For each of the simulations all values within each 2x2 degree grid cell each month were averaged to produce 1000 x 12 different monthly climatological grids of δ_A, surface temperature and normalized relative humidity (fourth row in **Figure S2**). Finally, because the strength of kinetic isotope fractionation effects are also uncertain, a different value of C_K was generated for each simulation, with this distribution assumed uniform between 2 and 6.5 [*Merlivat and Jouzel*, 1979] (fifth red box in **Figure S2**).

The gridded simulations for δ_A, surface temperature, relative humidity, and C_K values were all combined and used to calculate 1000 x 12 different grids of $\delta_{E(O)}$ using Equation (S2) (second purple diamond **Figure S2**). The $\delta_{E(O)}$ grids were then used with the bulk fluxes and precipitation isotope estimates to calculate 1000 global mass balance estimates using the equations descripted in **Text S3**. For the bulk fluxes of precipitation and oceanic evaporation, both observational uncertainty and inter-annual variability are considered via a resampling approach with random errors included. For each simulation, one of the years during the TES period (2005-2012) was selected at random (representing inter-annual variability in fluxes). Then based on the error assessment included with the GPCP and OAflux data files random noise was added to that years precipitation and evaporation fluxes (this incorporates any observations uncertaity). Although our study only considers the GPCP and OAFlux datasets, and other global flux data produces with somewhat different characteristics are available, the variability introduced in our analysis by resampling years at random (e.g. oceanic precipitation varies from 372,000 km^3 to 393,000 km^3) is larger than expected differences between different data products [*Syed et al.*, 2010].

The gridded precipitation and evaporation fluxes and their estimated isotope values are then combined to estimate the global fluxes with Equations (S3)-(S5) for each simulation (seventh row of **Figure S2**). Finally, these values were used in the ocean and atmosphere mass balance Equations (S6) and (S7) to determine the final value of continental runoff and evapotranspiration for each simulation. The mean and standard deviation of these simulations was then taken to determine the final value of $\overline{\delta_{R(L)}}$ and $\overline{\delta_{ET(L)}}$, and its associated uncertainty.

Figure S1

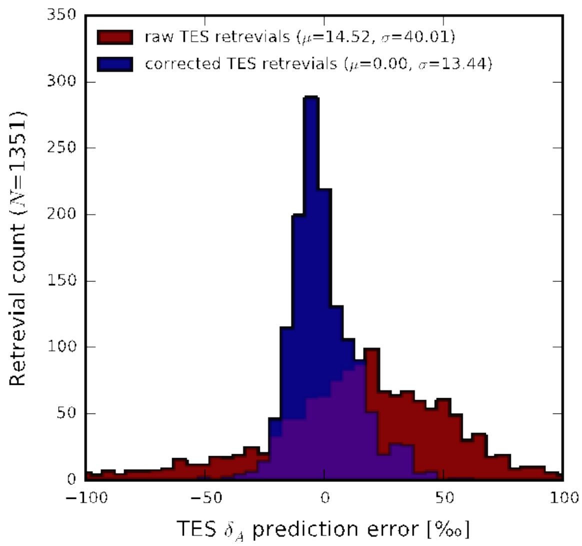

Figure S1. Difference between TES δ_A estimates and ship-based observations of atmospheric δ_A values based on jackknifed estimates of β coefficients ($\delta_{A(\mathrm{Error})} = \delta_{A(\mathrm{TES})}$ - $\delta_{A(\mathrm{Ship})}$).

Figure S2

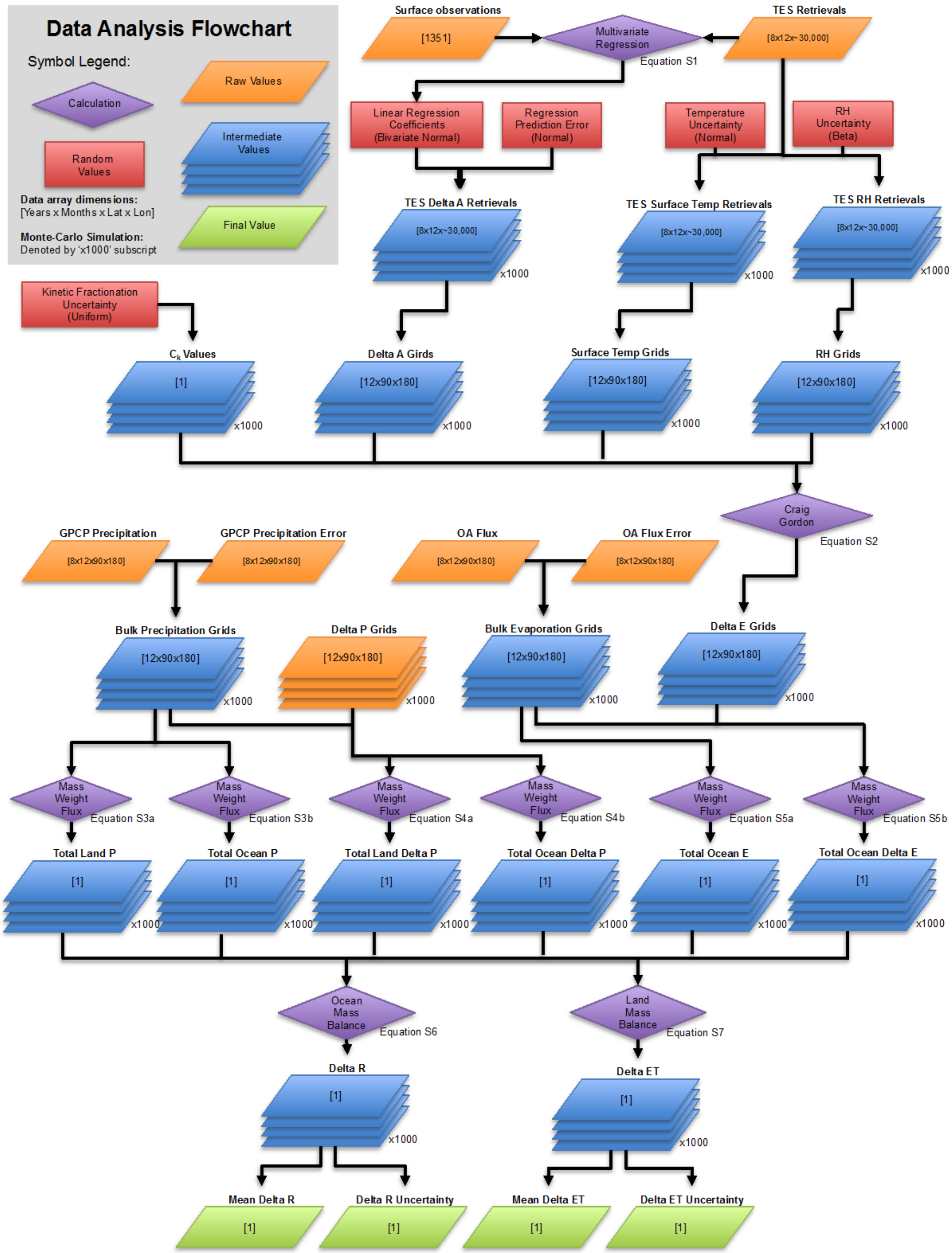

Figure S2. Flowchart depicting the data analysis steps used in this study.

Table S1

n	**Parameter (x_n)**	**Units**	β_n	σ_n	ρ_n *
1	TES surface δ_A retrieval	‰	4.60e-03	2.87e-04	0.50
2	TES troposphere δ_A retrieval	‰	9.91e-02	4.40e-04	0.02
3	TES surface δ_A a-priori	‰	3.68e-01	4.95e-03	0.29
4	TES troposphere δ_A a-priori	‰	-1.57e-01	6.52e-04	-0.65
5	TES surface q retrieval	mol/mol	-1.22e+02	2.05e+00	0.60
6	TES troposphere q retrieval	mol/mol	5.65e+02	9.68e+00	0.56
7	TES surface q a-priori	mol/mol	3.25e+03	6.57e+00	0.69
8	TES troposphere q a-priori	mol/mol	-6.87+03	1.75e+01	0.59
9	Intercept		-9.91e+01	4.07e-01	

*All regression coefficients are highly significant at $p<0.001$, except for x_2, where $p<0.5$.

Table S1. Meta-data parameters used to bias-correct TES surface retrievals.

Table S2

Rank	River	Flow[1] [$km^3\ yr^{-1}$]	δD [‰]	Reference
1	Amazon	6642	-46	[*Longinelli and Edmond*, 1983]
2	Congo	3699	-13	[*Vangriesheim et al.*, 2009]
4	Changjiang	944	-46	[*IAEA*, 2012]
5	Brahmaputra	628	-48	[*Gajurel et al.*, 2006]
6	Mississippi	610	-44	[*Kendall and Coplen*, 2001]
7	Yenisei	599	-139	[*Yi et al.*, 2012]
8	Parana	568	-33	[*Panarello and Dapeña*, 2009]
9	Lena	531	-156	[*Yi et al.*, 2012]
10	Mekong	525	-38	[*IAEA*, 2012]
12	Ob	412	-113	[*Yi et al.*, 2012]
14	St Lawrence	363	-52	[*Kendall and Coplen*, 2001]
17	Amur	354	-108	[*Moon et al.*, 2009]
19	Mackenzie	290	-154	[*Yi et al.*, 2012]
21	Columbia	252	-124	[*Kendall and Coplen*, 2001]
24	Yukon	212	-158	[*Yi et al.*, 2012]
26	Danube	202	-69	[*IAEA*, 2012]
30	Fraser	140	-136	[*Cameron et al.*, 1995]
35	Kolyma	118	-171	[*Yi et al.*, 2012]
38	Indus	104	-55	[*IAEA*, 2012]
49	Sacramento	69	-79	[*Kendall and Coplen*, 2001]
53	Kuskokwim	57	-132	[*Kendall and Coplen*, 2001]
67	Alabama	51	-24	[*Kendall and Coplen*, 2001]
68	Stikine	51	-139	[*Kendall and Coplen*, 2001]
74	Susquehanna	46	-56	[*Kendall and Coplen*, 2001]
77	Susitna	45	-151	[*Kendall and Coplen*, 2001]
95	Copper	34	-168	[*Kendall and Coplen*, 2001]
108	Nushagak	31	-113	[*Kendall and Coplen*, 2001]
123	Tombigbee	27	-23	[*Kendall and Coplen*, 2001]
165	Colorado	12	-99	[*Kendall and Coplen*, 2001]
179	Brazos	7	-19	[*Kendall and Coplen*, 2001]
194	Colorado (TX)	3	-19	[*Kendall and Coplen*, 2001]
195	Rio Grande	1	-12	[*Kendall and Coplen*, 2001]

[1]Flow at mouth and rank estimates from [*Dai and Trenberth*, 2002]

Table S2. Literature review of the D/H isotope ratio of rivers worldwide.

Table S3

Location	**δD Range** [‰]	**System**	**Reference**
Arizona, US	-79 to -74	Savanna	[*Yepez et al.*, 2003]
Morocco	-63 to -40	Olive orchard	[*Williams et al.*, 2004]
Arizona, US	-71 to +100	Savanna	[*Yepez et al.*, 2005]
China	-64 to -53	Shrubland	[*Xu et al.*, 2008]
Colorado, US	-150 to -290	Grassland	[*Noone et al.*, 2013]
Kenya	-75 to -40	Savanna	[*Good et al.*, 2014]

Table S3. Literature review of measured evapotranspiration D/H isotope ratios.

Data Set S1

Bias-corrected marine surface layer δ_A estimates and their uncertainty are included as a supplementary data file (sd01.nc).

Supporting Information References

Adler, R. F. et al. (2003), The Version-2 Global Precipitation Climatology Project (GPCP) Monthly Precipitation Analysis (1979–Present), *J. Hydrometeorol.*, *4*(6), 1147–1167, doi:10.1175/1525-7541(2003)004<1147:TVGPCP>2.0.CO;2.

Bowen, G. J., and J. Revenaugh (2003), Interpolating the isotopic composition of modern meteoric precipitation, *Water Resour. Res.*, *39*(10), 1–13, doi:10.1029/2003WR002086.

Bowen, G. J., and B. Wilkinson (2002), Spatial distribution of δ18O in meteoric precipitation, *Geology*, *30*(4), 315–318, doi:10.1130/0091-7613(2002)030<0315:SDOOIM>2.0.CO;2.

Cameron, E. M., G. E. M. Hall, J. Veizer, and H. R. Krouse (1995), Isotopic and elemental hydrogeochemistry of a major river system: Fraser River, British Columbia, Canada, *Chem. Geol.*, *122*(1-4), 149–169, doi:10.1016/0009-2541(95)00007-9.

Craig, H., and L. I. Gordon (1965), Deuterium and oxygen-18 variations in the ocean and the marine atmosphere, in *Stable Isotopes in Oceanographic Studies and Paleotemperatures*, edited by E. Tongiori, pp. 9–130, Consiglio Nazionale Delle Richerche Laboratorio Di Gelogica Nucleare, Pisa, Italy.

Dai, A., and K. E. Trenberth (2002), Estimates of Freshwater Discharge from Continents: Latitudinal and Seasonal Variations, *J. Hydrometeorol.*, *3*(6), 660–687, doi:10.1175/1525-7541(2002)003<0660:EOFDFC>2.0.CO;2.

Field, R. D., C. Risi, G. A. Schmidt, J. Worden, A. Voulgarakis, A. N. LeGrande, A. H. Sobel, and R. J. Healy (2012), A Tropospheric Emission Spectrometer HDO/H_2O retrieval simulator for climate models, *Atmos. Chem. Phys.*, *12*(21), 10485–10504, doi:10.5194/acp-12-10485-2012.

Gajurel, A. P., C. France-Lanord, P. Huyghe, C. Guilmette, and D. Gurung (2006), C and O isotope compositions of modern fresh-water mollusc shells and river waters from the Himalaya and Ganga plain, *Chem. Geol.*, *233*(1), 156–183, doi:10.1016/j.chemgeo.2006.03.002.

Gat, J. R. (1996), Oxygen and hydrogen isotopes in the hydrologic cycle, *Annu. Rev. Earth Planet. Sci.*, *24*(1), 225–262, doi:10.1146/annurev.earth.24.1.225.

Good, S. P., K. Soderberg, K. Guan, E. G. King, T. M. Scanlon, and K. K. Caylor (2014), δ2H isotopic flux partitioning of evapotranspiration over a grass field following a water pulse and subsequent dry down, *Water Resour. Res.*, *50*(DOI:10.1002/2013WR014333), 1410–1432, doi:10.1002/2013WR014333.Received.

Herman, R., and G. Osterman (2012), Earth Observing System (EOS) Tropospheric Emission Spectrometer (TES),

Horita, J., K. Rozanski, and S. Cohen (2008), Isotope effects in the evaporation of water: a status report of the Craig-Gordon model., *Isotopes Environ. Health Stud.*, *44*(1), 23–49, doi:10.1080/10256010801887174.

IAEA (2012), *Monitoring Isotopes In Rivers: Creation Of The Global Network Of Isotopes In Rivers (GNIR)*, IAEA-TECDOC-1673, International Atomic Energy Agency, Isotope Hydrology Section, Vienna, Austria.

Kendall, C., and T. B. Coplen (2001), Distribution of oxygen-18 and deuterium in river waters across the United States, *Hydrol. Process.*, *15*(7), 1363–1393, doi:10.1002/hyp.217.

Longinelli, A., and J. M. Edmond (1983), Isotope geochemistry of the Amazon Basin: A reconnaissance, *J. Geophys. Res.*, *88*(C6), 3703, doi:10.1029/JC088iC06p03703.

Majoube, M. (1971), Fractionnement en oxygene 18 et en deuterium entre leau et sa vapeur, *J. Chim. Phys*, *68*, 1423–1436.

Merlivat, L., and J. Jouzel (1979), Global climatic interpretation of the deuterium-oxygen 18 relationship for precipitation, *J. Geophys. Res.*, *84*(C8), 5029–5033, doi:10.1029/JC084iC08p05029.

Moon, S., Y. Huh, and A. Zaitsev (2009), Hydrochemistry of the Amur River: Weathering in a Northern Temperate Basin, *Aquat. Geochemistry*, *15*(4), 497–527, doi:10.1007/s10498-009-9063-6.

Noone, D. et al. (2013), Determining water sources in the boundary layer from tall tower profiles of water vapor and surface water isotope ratios after a snowstorm in Colorado, *Atmos. Chem. Phys.*, *13*(3), 1607–1623, doi:10.5194/acp-13-1607-2013.

Panarello, H. O., and C. Dapeña (2009), Large scale meteorological phenomena, ENSO and ITCZ, define the Parana River isotope composition, *J. Hydrol.*, *365*(1-2), 105–112, doi:10.1016/j.jhydrol.2008.11.026.

Syed, T. H., J. S. Famiglietti, D. P. Chambers, J. K. Willis, and K. Hilburn (2010), Satellite-based global-ocean mass balance estimates of interannual variability and emerging trends in continental freshwater discharge., *Proc. Natl. Acad. Sci. U. S. A.*, *107*(42), 17916–21, doi:10.1073/pnas.1003292107.

Vangriesheim, A., C. Pierre, A. Aminot, N. Metzl, F. Baurand, and J.-C. Caprais (2009), The influence of Congo River discharges in the surface and deep layers of the Gulf of Guinea, *Deep Sea Res. Part II Top. Stud. Oceanogr.*, *56*(23), 2183–2196, doi:10.1016/j.dsr2.2009.04.002.

Williams, D. G. et al. (2004), Evapotranspiration components determined by stable isotope, sap flow and eddy covariance techniques, *Agric. For. Meteorol.*, *125*(3-4), 241–258, doi:10.1016/j.agrformet.2004.04.008.

Wu, C.-F. J. (1986), Jackknife, bootstrap and other resampling methods in regression analysis, *Ann. Stat.*, *14*(4), 1261–1295.

Xu, Z., H. Yang, F. Liu, S. An, J. Cui, Z. Wang, and S. Liu (2008), Partitioning evapotranspiration flux components in a subalpine shrubland based on stable isotopic measurements, *Bot. Stud.*, *49*(4), 351–361.

Yepez, E. A., D. G. Williams, R. L. Scott, and G. Lin (2003), Partitioning overstory and understory evapotranspiration in a semiarid savanna woodland from the isotopic composition of water vapor, *Agric. For. Meteorol.*, *119*(1-2), 53–68.

Yepez, E. A., T. E. Huxman, D. D. Ignace, N. B. English, J. F. Weltzin, A. E. Castellanos, and D. G. Williams (2005), Dynamics of transpiration and evaporation following a moisture pulse in semiarid grassland: a chamber-based isotope method for partitioning flux components, *Agric. For. Meteorol.*, *132*(3-4), 359–376.

Yi, Y., J. J. Gibson, L. W. Cooper, J.-F. Hélie, S. J. Birks, J. W. McClelland, R. M. Holmes, and B. J. Peterson (2012), Isotopic signals (18 O, 2 H, 3 H) of six major rivers draining the pan-Arctic watershed, *Global Biogeochem. Cycles*, *26*(1), n/a–n/a, doi:10.1029/2011GB004159.

Yu, L., and R. A. Weller (2007), Objectively Analyzed Air–Sea Heat Fluxes for the Global Ice-Free Oceans (1981–2005), *Bull. Am. Meteorol. Soc.*, *88*(4), 527–539, doi:10.1175/BAMS-88-4-527.